Investigation of optical parametric fluorescence suppression with a quencher pulse in an optical parametric chirped-pulse amplification laser

Japanese Journal of Applied Physics **57**, 012701 (2018)
https://doi.org/10.7567/JJAP.57.012701

REGULAR PAPER

Investigation of optical parametric fluorescence suppression with a quencher pulse in an optical parametric chirped-pulse amplification laser

Zhaoyang Li*, Shogo Tomita, Toshikazu Uesu, and Noriaki Miyanaga*

Institute of Laser Engineering, Osaka University, Suita, Osaka 565-0871, Japan

*E-mail: zhaoyang-li@ile.osaka-u.ac.jp; miyanaga@ile.osaka-u.ac.jp

Received September 12, 2017; accepted October 26, 2017; published online December 1, 2017

The mechanism of suppressing optical parametric fluorescence (OPF) with a quencher pulse in an optical parametric chirped-pulse amplification (OPCPA) laser is investigated. A simplified theoretical model of this phenomenon is presented, and numerical simulations and experimental demonstrations are performed for explanation and verification. The results show that, although the improvement of the temporal contrast usually is limited, the generation and amplification of the OPF in an OPCPA process does be suppressed by the injection of a quencher pulse, and the suppression capability can be slightly enhanced by increasing the quencher-pulse energy. We believe that this work will be helpful in designing high-peak-power lasers with high temporal contrast.

1. Introduction

In the last two decades, high-field laser physics and potential applications have accelerated the development of petawatt (PW, 10^{15} W) lasers.[1,2] Since the demonstration of the first PW laser in the Nova system at the Lawrence Livermore National Laboratory in 1996,[3] several PW lasers with femtosecond/picosecond pulse durations and hundred/thousand Joule pulse energies have been realized in various laboratories.[3–8] In addition, several 10-PW lasers, such as Extreme Light Infrastructure (ELI)[9] and Apollon-10-PW,[10] are currently being constructed. Furthermore, two exawatt (EW, 10^{18} W) laser facilities, with peak power of up to 0.2 EW,[11,12] are in the planning stage. Chirped-pulse amplification (CPA),[13] optical parameter amplification (OPA), and optical parametric chirped-pulse amplification (OPCPA)[14] are widely used in engineering fields to obtain a high peak power. The subsequent step, i.e., the stimulated Raman backscattering in plasma, is considered an alternative method for further pulse amplification and compression.[15] For a high-peak-power laser, the temporal contrast is a key parameter, which directly determines the final applications thereof. For example, the peak power of the pre-pulse or pedestal of a 1-PW laser with a temporal contrast of 10^{-6} is 10^9 W. This pre-pulse/pedestal can generate low-density preplasma and destroy the experimental target before the main interaction pulse arrives. In the past decade, several attempts have been aimed at improving this key parameter for PW lasers worldwide. Unfortunately, the temporal contrast of a CPA/OPCPA laser is influenced by many factors, including the oscillator itself,[16] spectral phase distortion,[17–20] spectral amplitude modulation,[21,22] amplified spontaneous emission (ASE),[23] OPF (or amplified OPF, i.e., AOPF, or superfluorescence),[24–28] scattering pulses,[29] etc., and is therefore very complex. Several methods for improvement, including low-gain OPCPA/OPA,[30] asymmetrical OPF,[31] cross-polarized wave generation,[32] frequency doubling,[33] self-diffraction,[34] picosecond OPCPA/OPA,[35] saturable absorption,[36,37] phase-conjugate wave generation,[38] interference modulation,[39] etc., have been proposed. However, PW lasers worldwide still suffer from the problem of relatively low temporal contrast, especially for Nd:glass CPA laser system.

Most recently designed PW lasers have been based on the technique of OPCPA, which boasts several advantages, including broad bandwidth, high gain, low dispersion, and weak thermal effect. However, this technique suffers from a major drawback, i.e., OPF, which further degrades the temporal contrast. Several investigations have focused on identifying OPF-related problems,[24,25] and several novel methods have been proposed for OPF suppression[26,27] or filtering.[28] In 2006, Kondo et al. proposed a quenching method [see Fig. 1(a)] for controlling OPF generated from the OPCPA stage in a Ti:sapphire CPA system by injecting a quencher (additional fundamental) pulse.[27] In their experimental demonstration, the OPF was suppressed during

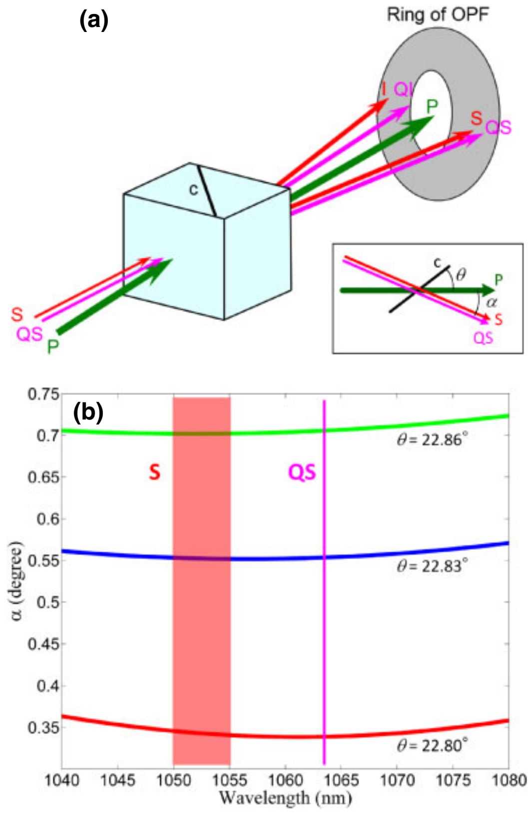

Fig. 1. (Color online) (a) Configuration of non-collinear phase-matching in a uniaxial non-linear crystal, when a quencher pulse is injected. (b) Non-collinear angle α as a function of wavelength for various phase-matching angles θ. S: signal, I: idler, P: pump, QS: quencher signal, QI: quencher idler, and c: optic axis.

injection of the quencher pulse. The corresponding output energy (mainly from OPF) decreased with increasing quencher energy, in the absence of incident seed to the laser system. This indicates that the temporal contrast should be improved further with increasing quencher-pulse energy. However, a theory for ASE in a CPA laser, instead of optical parametric process in an OPA/OPCPA laser, was used to explain this phenomena. Therefore, in this work, a simplified theoretical model based on five-wave coupled wave equations with added quantum noise components is proposed for explaining and optimizing the quenching method. Theoretical simulations and corresponding experimental demonstrations are performed. The major objective of this work is to re-explain this phenomenon and further optimize the quenching method for OPCPA/OPA lasers, which must fulfill high temporal-contrast requirements.

2. Simplified theoretical model and simulation

An OPF-involved OPA/OPCPA process obeys the coupled wave equations, when the quantum noise field terms are considered. A complex Gaussian stochastic variable $\xi_\mathrm{i}(z,t)$, with a zero mean $\langle \xi_\mathrm{i}(z,t)\rangle = 0$ and the correlation $\langle \xi_\mathrm{i}(z,t)\xi_\mathrm{j}^*(z',t')\rangle = \delta_{\mathrm{i,j}}\delta(t-t')\delta(z-z')$, is generally used to describe the quantum noise components. This description of noise, i.e., via classical-type Langevin equations, was first introduced by Gatii et al.[40,41] In a PW laser, the non-linearity in the amplification beamline is typically reduced by stretching the pulse duration to a nanosecond level. In this case, to simplify our theoretical model, various effects (including the group velocity, dispersion, diffraction, spatial walk-off, loss, and coupling between signal and quencher) are neglected and, hence, for the perfect phase-matching (i.e., $\Delta k = 0$) the coupled wave equations can be expressed as

$$\begin{aligned}
\frac{\partial A_1}{\partial z} &= \frac{2id_\mathrm{eff}\omega_1}{n_1 c}A_2^*A_3 + A_1^\mathrm{q},\\
\frac{\partial A_2}{\partial z} &= \frac{2id_\mathrm{eff}\omega_2}{n_2 c}A_1^*A_3 + A_2^\mathrm{q},\\
\frac{\partial A_3}{\partial z} &= \frac{2id_\mathrm{eff}\omega_3}{n_3 c}(A_1A_2 + A_4A_5) + A_3^\mathrm{q},\\
\frac{\partial A_4}{\partial z} &= \frac{2id_\mathrm{eff}\omega_4}{n_4 c}A_5^*A_3 + A_4^\mathrm{q},\\
\frac{\partial A_5}{\partial z} &= \frac{2id_\mathrm{eff}\omega_5}{n_5 c}A_4^*A_3 + A_5^\mathrm{q},
\end{aligned} \tag{1}$$

where, A_i ($i = 1$, 2, 3, 4, and 5): complex amplitudes of the signal (or the OPF field in the signal direction), idler (or the OPF field in the idler direction), pump, quencher signal (or the OPF field in the quencher signal direction), and quencher idler (or the OPF field in the quencher idler direction), d_eff: effective nonlinear coefficient, A_i^q: quantum noise components of each field A_i. Moreover, the angular frequencies ω_i are related as follows: $\omega_1 + \omega_2 = \omega_3$ and $\omega_4 + \omega_5 = \omega_3$. The perfect phase-matching can be obtained by optimizing the geometry of the parametric process. Here we consider OPCPA front end in Nd:glass CPA system, where the signal wavelength is 1053 nm. The pump laser is the second harmonic (532 nm wavelength) of Nd:YAG laser, and the quencher is the fundamental wave (1064 nm). Figure 1(b) shows the non-collinear angle α (inside beta barium borate, BBO) in type I BBO crystal as a function of signal wavelength with a parameter of phase-matching angle θ (inside BBO). Taking an appropriate non-collinear angle $\alpha = 0.55°$ (inside BBO), the almost perfect phase-matching condition can be realized for both 1053 nm signal and 1064 nm quencher. In Eq. (1), for simplification, the stochastic variable $\xi_\mathrm{i}(z,t)$ is assumed to be unity and, therefore the probability of generating quantum noise components A_i^q is 100%. This hypothesis is reasonable in the case of a strong pump. In our model, a linear dependency is assumed for the relationship between the intensity of the pump and the intensity of the quantum noise field A_i^q ($i = 1$, 2, 4, and 5) in the direction of the signal, idler, quencher signal, and quencher idler. Furthermore, the intensity of A_3^q is set to zero as the pump field is already initialized with the complex amplitude. And meanwhile, quantum noises in other spatial directions (i.e., other wavelengths) are neglected for further simplification.

Table I. Parameters used in the simulation.

Crystal	Type I BBO with perfect phase matching			
	Signal	Pump	Quencher	Quantum noise
Wavelength	1053 nm	532 nm	1064 nm	—
Duration	2.5 ns	5 ns	5 ns	5 ns
Energy	0/6 μJ	100 mJ	0/2 μJ	1 nJ
Diameter	2 mm	2 mm	2 mm	2 mm
Peak intensity	~0/76 kW/cm^2	~637 MW/cm^2	~0/13 kW/cm^2	~6.4 W/cm^2

Using Eq. (1), the pulse-energy evolution (with and without a quencher pulse) along the propagation direction is simulated using the following parameters of pump, i.e., wavelength: 532 nm, pulse energy: 100 mJ, pulse duration: 5 ns, and beam diameter: 2 mm. The parameters correspond to the incident signal and injected quencher signal, respectively, are as follows, center wavelength: 1053 and 1064 nm, pulse energy: 6 and 2 μJ, pulse duration: 2.5 and 5 ns. The beam diameter was 2 mm in both cases. The intensity spatial distribution is assumed to be a flat-top profile for simplification. According to previous studies, the intensity of each quantum noise field A_i^q ($i = 1$, 2, 4, and 5) should be chosen empirically.[24] In this work, we assume that the pulse duration is equal to that of the pump, and the pulse energy is 1 nJ. Actually, this pulse energy can be adjusted according to various real conditions, and we won't discuss it here in detail. Thereby, the simulation parameters are listed in Table I.

The simulation is performed to consider four types of cases applied to a type I phase-matching BBO crystal. In the first case, a 6-μJ incident signal without a quencher pulse, denoted by red lines in Fig. 2(a), is considered. The energy of the signal and idler increases along the propagation direction, and the peak energy occurs at ~15 mm, corresponding to the position of zero pump energy. In the second case, a 2-μJ quencher signal is injected, denoted by blue lines in Fig. 2(a), and the energy of the signal, idler, quencher signal, and quencher idler increases with increasing length of the BBO crystal. The peak energy also occurs at ~15 mm along the crystal. However, compared with the first case, the energy of the amplified signal is lower, because the injected quencher pulse induces some of the pump energy transferred to the amplified quencher signal and its idler. To investigate the characteristics of OPF, we set the incident signal to zero. The third and fourth cases correspond to scenarios without and

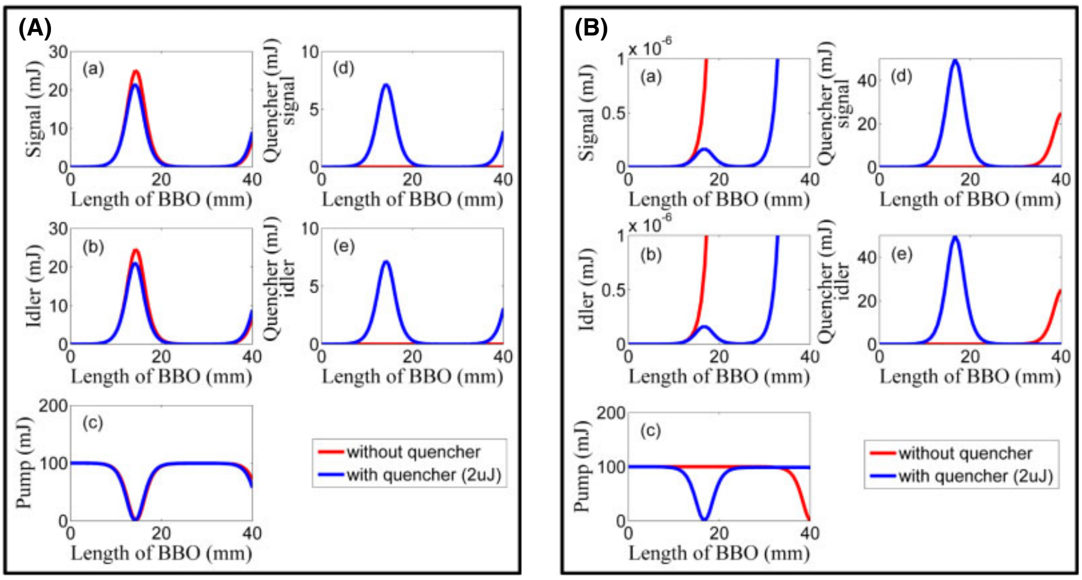

Fig. 2. (Color online) Pulse energy in the (1) signal, (2) idler, (3) pump, (4) quencher signal, and (5) quencher idler direction as a function of the BBO length. The incident signal has an energy of (a) 6 μJ and (b) 0 μJ. Red and blue lines denote the results obtained for a pulse without and with a 2-μJ quencher signal, respectively.

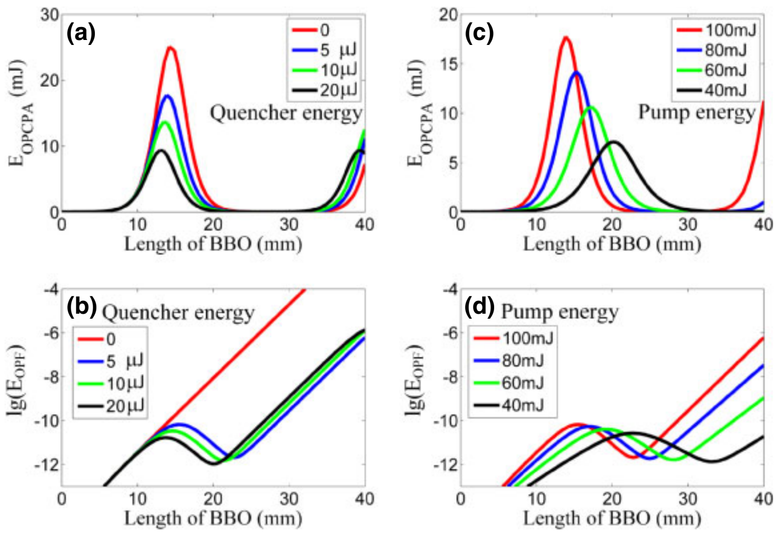

Fig. 3. (Color online) (a, c) E_{OPCPA} and (b, d) common logarithmic (lg) plot of E_{OPF} as a function of the BBO length for variations in the (a, b) quencher energy and (c, d) pump energy. The energy of the (a, c) incident signal is 6 μJ, (a, b) pump is 100 mJ, and (c, d) quencher signal is 5 μJ.

with a quencher pulse, respectively. For the third case, denoted by red lines in Fig. 2(b), OPF in the signal, idler, quencher signal, and quencher idler directions increase monotonously within the simulation range. Injection of a 2-μJ quencher signal (i.e., the fourth case) yields an initial monotonous increase (see blue lines in the figure). This is followed by a decrease in OPF in the signal and idler directions at ∼17 mm, where peak energies of both the quencher signal and its idler occur. The monotonous increase in the OPF is changed by the transfer of energy from the quencher signal and its idler back to the pump, indicating that the OPF in an OPCPA/OPA can be suppressed by a quencher pulse. Moreover, non-zero signals would lead to further suppression of OPF. However, the change of the result shown in Fig. 2(b) would be small, and the overall evolution will remain unchanged.

When pulse durations and beam diameters in Table I are fixed, we also determine the influence of the quencher energy (i.e., intensity) and the pump energy (i.e., intensity) on OPF suppression. Here, we use E_{OPCPA} and E_{OPF} to represent the energy in the signal direction with and without an incident signal, respectively. Figures 3(a) and 3(b) show the evolution, with quencher energy, of E_{OPCPA} and E_{OPF} along the length of the crystal. The tendency of simulation results can be summarized at a glance as follows. (i) E_{OPCPA} and E_{OPF} both decrease with increasing quencher energy [see Figs. 3(a) and 3(b)] for a pump energy of 100 mJ, and they both decrease with decreasing pump energy [see Figs. 3(c) and 3(d)] for an injected quencher-signal energy of 5 μJ. (ii) Comparing Figs. 3(a) and 3(c) with Figs. 3(b) and 3(d), respectively, for different quencher and pump energies, it is apparent that E_{OPCPA} has a maximum at a certain crystal length near the first peak associated with E_{OPF} and the corresponding crystal length is inversely proportional to the quencher energy and the pump energy. Therefore, for an optimum crystal length, both E_{OPCPA} and E_{OPF} change when

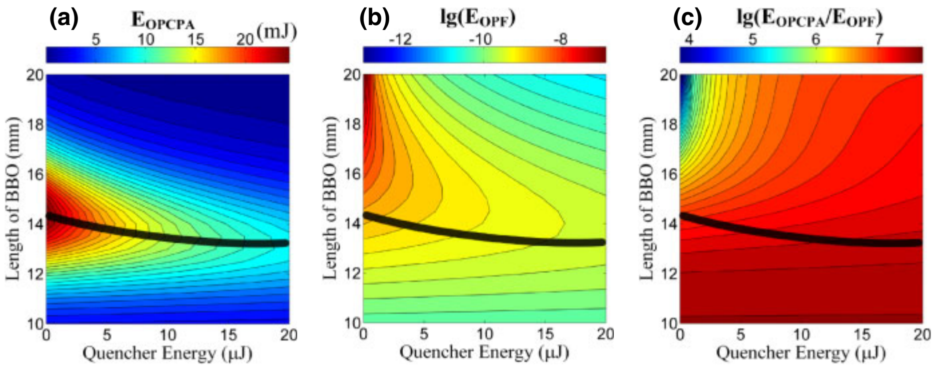

Fig. 4. (Color online) Evolution of (a) E_{OPCPA}, (b) common logarithmic (lg) plot of E_{OPF}, and (c) common logarithmic (lg) plot of E_{OPCPA}/E_{OPF} with BBO length and the quencher energy, for a fixed pump energy and incident-signal (for E_{OPCPA}) energy of 100 mJ and 6 μJ, respectively. The thick black lines show the position of the contour ridge of E_{OPCPA}.

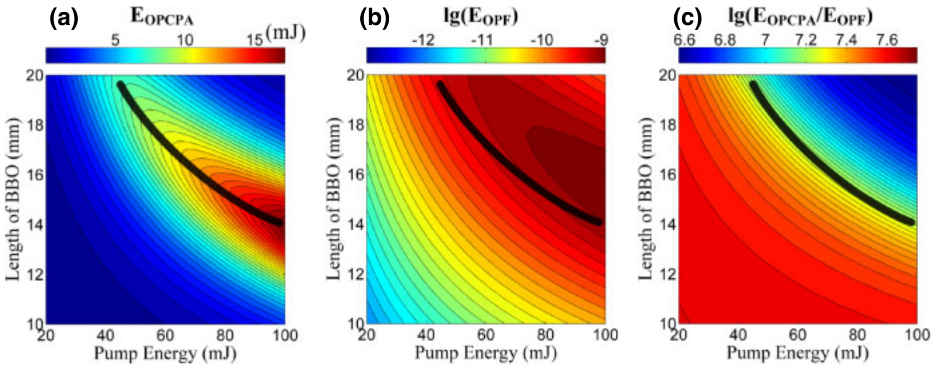

Fig. 5. (Color online) Evolution of (a) E_{OPCPA}, (b) common logarithmic (lg) plot of E_{OPF}, and (c) common logarithmic (lg) plot of E_{OPCPA}/E_{OPF} with the BBO length and the pump energy, for a quencher-signal energy and incident-signal (for E_{OPCPA}) energy of 5 and 6 μJ, respectively. The thick black lines show the position of the contour ridge of E_{OPCPA}.

we adjust the quencher and/or pump energy (i.e., intensity), rendering the estimation of the temporal-contrast evolution difficult.

In this case, we define a ratio of E_{OPCPA}/E_{OPF} and calculate the two-dimensional evolution of E_{OPCPA}, E_{OPF}, and their ratio E_{OPCPA}/E_{OPF} with the quencher energy and the BBO length. Figures 4(a) and 4(b) show that both E_{OPCPA} and E_{OPF} decrease with increasing quencher energy, whereas E_{OPCPA}/E_{OPF} increases. Thick black lines denote the position where the highest E_{OPCPA} for each injected quencher signal is achieved. Along this line, if the quencher energy is increased, E_{OPCPA}/E_{OPF} could increase (i.e., OPF suppression could be enhanced) [see Fig. 4(c)], although E_{OPCPA} (i.e., the amplified signal) would decrease [see Fig. 4(a)]. Therefore, to a certain extent, a strong quencher pulse is recommended for the design of a high temporal-contrast OPA/OPCPA frontend of a PW laser.

When the injected quencher signal is fixed at 5 μJ, the two-dimensional evolution of E_{OPCPA}, E_{OPF}, and their ratio E_{OPCPA}/E_{OPF} with the pump energy and the BBO length is simulated (see Fig. 5). Figure 5(a) shows that the highest possible E_{OPCPA} increases and the corresponding BBO length decreases with increasing pump energy. This concurs with the previous results. Similarly, Figs. 5(b) and 5(c) show that, along the thick black lines [which denote the contour ridge of E_{OPCPA} in Fig. 5(a)], E_{OPF} and E_{OPCPA}/E_{OPF} increase with increasing pump energy. However, in Fig. 5(c) this line is almost parallel to the contour line, importantly, indicating that (in this case) the ratio E_{OPCPA}/E_{OPF} (i.e., the pulse contrast) is less sensitive to the pump energy. Therefore, in an ideal case, varying the pump energy yields only modest improvements in OPF suppression.

The above simulation results suggest that OPF suppression in an OPA/OPCPA laser would appear while the quenching method is introduced, which should be further improved by increasing the injected quencher energy. Moreover, in the case of high-gain (e.g., at the first OPA/OPCPA stage in a frontend), the pump energy/intensity has relatively small influence on this OPF suppression theoretically.

3. Experimental demonstration

To verify the above described simulation, a simple demonstration was performed using an output from the pre-amplifier of our recently upgraded HALNA laser system.[42,43] During this demonstration, as shown in Fig. 6, a ∼110-fs seed pulse centered at 1053 nm was generated by an in-house-developed Yb-doped fiber mode-locking oscillator. The pulse duration was temporally stretched to ∼4.5 ns using a four-pass Offner grating stretcher, and the spectrum bandwidth was clipped to only ∼5 nm due to a limited grating size. Afterwards, the pulse energy was amplified to tens of micro-joule using a LD-pumped $Yb:CaF_2$ regenerative amplifier, and the pulse duration was narrowed to ∼2.5 ns due to the gain-narrowing effect. The pulse was then delivered to a 12-mm (length) type I BBO crystal for secondary amplification. A 532-nm pump pulse, with a pulse duration of ∼5 ns and a tunable pulse energy, was supplied by a Q-switched Nd:YAG laser (Continuum Surelite). The residual fundamental (wavelength:

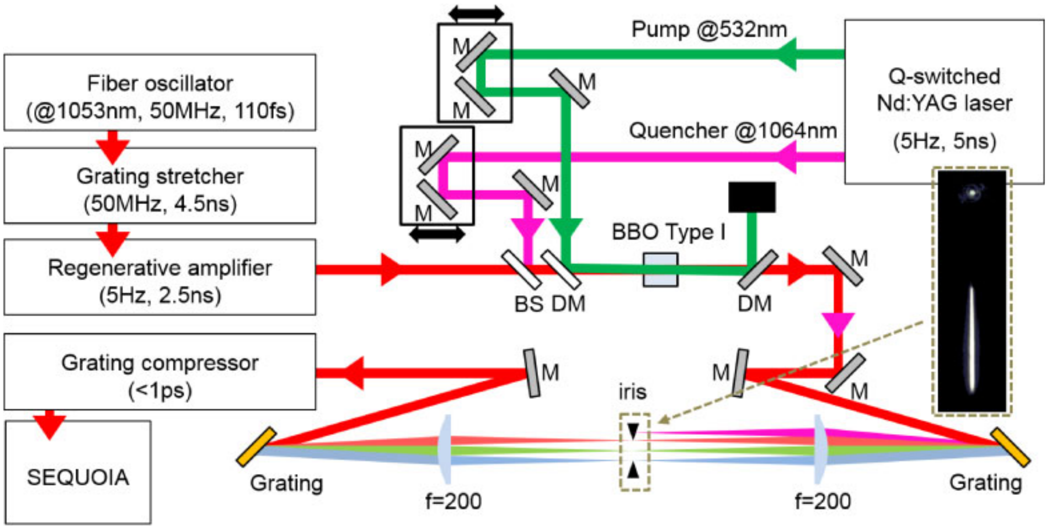

Fig. 6. (Color online) Experimental setup for the demonstration. The signal pulse originated from a CPA laser, and the quencher and pump pulses originated from a Q-switched Nd:YAG laser. The inset shows the CCD-captured beam pattern at the Fourier plane. BS: beam splitter and DM: dichroic mirror.

Table II. Parameters of the OPCPA stage used in the demonstration.

Crystal	12 mm type I BBO, 0.55° non-collinear angle (inside BBO)		
	Signal	Pump	Quencher
Wavelength	2.8 nm bandwidth at 1053 nm	532 nm	1064 nm
Duration	2.5 ns	5 ns	5 ns
Energy	6 μJ	10–130 mJ	0–10 μJ
Diameter	5 mm	4 mm	4 mm
Peak intensity	~12 kW/cm^2	~16–207 MW/cm^2	~0–16 kW/cm^2

1064 nm, pulse duration: 5 ns) was used as the quencher pulse. The residual pump and the generated idler and quencher idler were removed via non-collinear phase-matching, with a non-collinear angle of ~0.55° (inside the BBO) between the signal and the pump. The signal and pump/quencher beams possess near Gaussian and super-Gaussian spatial profiles, respectively. And, the beam diameter of the signal, pump, and quencher signal at the BBO crystal was ~5, ~4, and ~4 mm, respectively. The main parameters of the OPCPA stage in our demonstration are listed in Table II. After the secondary amplification (i.e., OPCPA stage), the signal was separated from the quencher signal by aligning a grating-based 4f system (grating density: 1200 groove/mm, incident angle: 45°, focal length: 200 mm). The inset photo shows the beam pattern captured by a CCD camera at the Fourier plane. Owing to angular dispersion, a linear shape was obtained for the focal pattern of the broadband signal. The signal was completely separated from the quencher signal in space, and, hence, was conveniently extracted by introducing an iris at the Fourier plane. In the final step, the temporal chirp of the amplified signal was completely removed by a two-pass Treacy grating compressor. The corresponding temporal contrast was measured using a commercial third-order cross-correlator (Amplitude Technologies Sequoia).

During the experiment, the input signal at the OPCPA stage was 6 μJ, and the pulse energy of the pump and the quencher signal was increased from 10 to 130 mJ and from 0 to 10 uJ, respectively. Figure 7 shows that the output energy and gain of both the signal and the quencher signal increased with increasing pump energy. Figure 7(a) shows that the output energy and the gain of the signal decreased with increasing energy of the injected quencher signal. Figure 7(b) shows that the gain of the quencher signal decreased with increasing energy of the injected quencher signal, whereas the output energy increased. This is attributed to part of the output quencher signal arising directly from the input. A comparison of Fig. 7(a) with Figs. 4(a) and 5(a), suggests that the energy and the gain of the output signal would both decrease with a strong quencher signal, but increase with a strong pump. Here, the gain of the quencher signal [see Fig. 7(b)] was considerably higher than that of the signal [see Fig. 7(a)]. This results from the pulse duration of the quencher signal and the signal being the same as and only half of that of the pump, respectively.

The temporal contrast of the compressed signal was then measured for different cases. When the energy of the injected quencher signal was adjusted to 0, 6, and 10 μJ, Figs. 8(a) and 8(b) show the temporal contrasts measured at pump energy of 130 and 105 mJ, respectively. The black line in Figs. 8(a) and 8(b) is a reference obtained without the OPCPA stage (i.e., compression pulse of the output of the regenerative amplifier) which represents the temporal contrast with perfect OPF suppression. For the degradation of the black line itself, we suppose it is mainly induced by the ASE, as well as the pre- and post-pulses, in the regenerative amplifier. The transmission plates of the regenerative amplifier would produce post-pulses, and the amplitude temporal interference and the refractive index non-linearity shifted post-pulses to pre-pulses in the time domain.[44] Colored lines in Fig. 8 reveal severe OPF-induced degradation in the temporal contrast due to strong pumps. A comparison of red and green lines reveals that injection of a 6 μJ quencher pulse resulted in an improvement of the temporal contrast, indicating that the OPF was suppressed by this pulse. As shown by the blue line in Fig. 8(a), when the quencher pulse was increased from 6 to 10 μJ, the temporal contrast was slightly further enhanced. However, the enhancement of the temporal contrast in Fig. 8(b) by increasing the energy of the quencher pulse

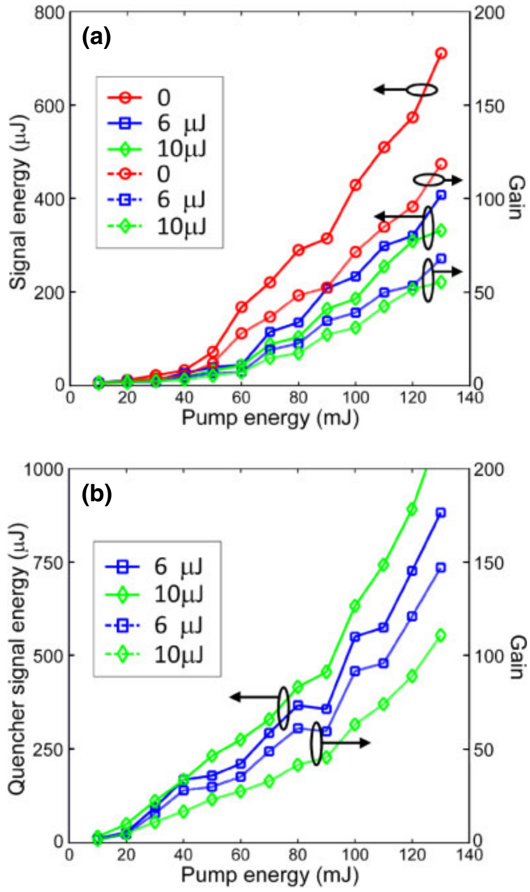

Fig. 7. (Color online) Dependence of the energy and the gain of the (a) signal and (b) quencher signal on the pump energy for various incident quencher energies.

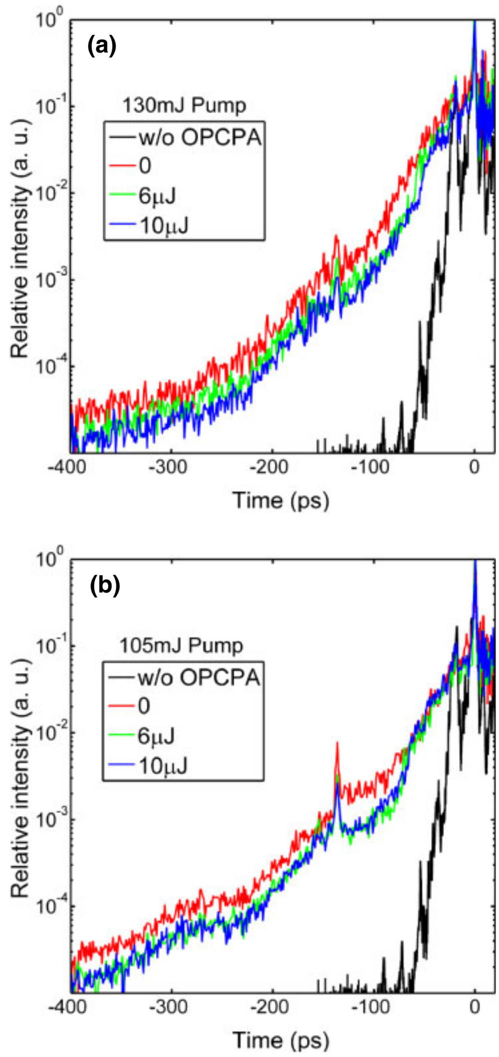

Fig. 8. (Color online) Measured temporal contrast taken with various quencher energies. Pump energies were (a) 130 and (b) 105 mJ, respectively. The energy of the incident signal was 6 µJ.

was not obvious. This result agrees with the simulation in Fig. 4: $E_{\mathrm{OPCPA}}/E_{\mathrm{OPF}}$ could increase with increasing the energy of the quencher pulse, however the sensitivity is very low. Furthermore, in our demonstration, the pre-pulse occurring near around −135 ps before the signal (see Fig. 8) is correlated with the post-pulse generated by the secondary reflection of the un-coating input and output surfaces of the 12-mm (length) BBO crystal, and the formation mechanism also includes the amplitude temporal interference and the refractive index non-linearity.

The simulation and demonstration suggest that the OPF-induced degradation of the temporal contrast can be reduced by injecting a quencher pulse, and which should be further improved by increasing the energy of the quencher pulse. However, the further improvement in experiments generally is very limited. In addition, Fig. 7 shows that the output energy or gain of the signal also decreases with increasing energy of the quencher pulse. In this condition, the energy of the quencher pulse associated with a real laser system should therefore be carefully adjusted, to achieve balance between OPF suppression and signal amplification.

4. Discussion

According to previous works, for the consideration of temporal contrast, a short crystal length with a low-gain is strongly suggested to control the generation and amplification of OPF.[23,29] In such OPA/OPCPA, we believe the improvement of the quenching method might be very limited and even can be neglected. However, sometimes, a long crystal and/or a high-gain (strong pump) are required in actual experiments (just like our demonstration experiment conditions), in this case the OPF-induced temporal contrast degradation could be slightly improved by injecting a quencher pulse. And the best improvement result should be achieved by optimizing the energy/intensity of the quencher pulse. Especially, in the case of multiple stages of OPA/OPCPA, we believe that the capability of this method would become obvious.

Furthermore, we should emphasize that, during our demonstration, the time delay between the pump and the signal was fixed, and then whose influence on the OPF-induced temporal contrast was removed. Moreover, the amplified spectrum, the compressed duration and the focal spot of the final outputs were monitored during the entire experiment, which possessed no significant changes, and accordingly the quenching method has no adverse influence on the majority parameters of signal pulses.

5. Conclusions

We have proposed a simplified five-wave coupled wave equations, considering quantum noise components, to explain the quenching method for OPF suppression in an OPA/OPCPA process. The simulation result shows that OPF suppression is induced mainly by the amplification of the quencher pulse and the transfer of energy from the quencher signal and its idler back to the pump. The theoretical prediction based on the simulation and the corresponding experimental demonstration show that OPF suppression could be obtained by injecting a quencher pulse. And, in theory, it should be further enhanced by increasing the quencher energy, however the sensitivity is not high. As a drawback, the output energy or the gain of the signal would decrease with increasing quencher energy and, hence, OPF suppression and signal amplification should be carefully balanced in an actual design. Although the temporal contrast improvement of the quenching method is generally limited, we believe this work still proves useful for high-peak-power (e.g., PW and EW) lasers, especially lasers with multiple stages of OPA/OPCPA.

Acknowledgments

This work was supported by Japan Society for the Promotion of Science Grants-in-Aid for Scientific Research (KAKENHI JP25247096). The authors gratefully acknowledge Dr. K. Tsubakimoto, Dr. Y. Nakata and Mr. H. Yoshida for helpful discussions, and Dr. S. Tokita, Dr. T. Kurita, Dr. K. Teramoto, Mr. S. Matsuo, and Mr. T. Terao for their contributions to upgrading the HALNA laser system.

1) J. D. Zuegel, S. Borneis, C. Barty, B. Legarrec, C. Danson, N. Miyanaga, P. K. Rambo, C. Leblanc, T. J. Kessler, A. W. Schmid, L. J. Waxer, J. H. Kelly, B. Kruschwitz, R. Jungquist, E. Moses, J. Britten, I. Jovanovic, J. Dawson, and N. Blanchot, Fusion Sci. Technol. **49**, 453 (2006).
2) C. Danson, D. Hillier, N. Hopps, and D. Neely, High Power Laser Sci. Eng. **3**, e3 (2015).
3) M. D. Perry, D. Pennington, B. C. Stuart, G. Tietbohl, J. A. Britten, C. Brown, S. Herman, B. Golick, M. Kartz, J. Miller, H. T. Powell, M. Vergino, and V. Yanovsky, Opt. Lett. **24**, 160 (1999).
4) M. Aoyama, K. Yamakawa, Y. Akahane, J. Ma, N. Inoue, H. Ueda, and H. Kiriyama, Opt. Lett. **28**, 1594 (2003).
5) N. Miyanaga, H. Azechi, K. A. Tanaka, T. Kanabe, T. Jitsuno, J. Kawanaka, Y. Fujimoto, R. Kodama, H. Shiraga, K. Knodo, K. Tsubakimoto, H. Habara, J. Lu, G. Xu, N. Morio, S. Matsuo, E. Miyaji, Y. Kawakami, Y. Izawa, and K. Mima, J. Phys. IV **133**, 81 (2006).
6) Y. Chu, X. Liang, L. Yu, Y. Xu, L. Xu, L. Ma, X. Lu, Y. Liu, Y. Leng, R. Li, and Z. Xu, Opt. Express **21**, 29231 (2013).
7) J. Sung, H. Lee, J. Yoo, J. Yoon, C. Lee, J. Yang, Y. Son, Y. Jang, S. Lee, and C. Nam, Opt. Lett. **42**, 2058 (2017).
8) X. Zeng, K. Zhou, Y. Zuo, Q. Zhu, J. Su, X. Wang, X. Wang, X. Huang, X. Jiang, D. Jiang, Y. Guo, N. Xie, S. Zhou, Z. Wu, J. Mu, H. Peng, and F. Jing, Opt. Lett. **42**, 2014 (2017).
9) D. Powell, Nature **500**, 264 (2013).
10) J. P. Zou, C. Le Blanc, D. N. Papadopoulos, G. Chériaux, P. Georges, G. Mennerat, F. Druon, L. Lecherbourg, A. Pellegrina, P. Ramirez, F. Giambruno, A. Fréneaux, F. Leconte, D. Badarau, J. M. Boudenne, D. Fournet, T. Valloton, J. L. Paillard, J. L. Veray, M. Pina, P. Monot, J. P. Chambaret, P. Martin, F. Mathieu, P. Audebert, and F. Amiranoff, High Power Laser Sci. Eng. **3**, e2 (2015).
11) G. A. Mourou, G. Korn, W. Sandner, and J. L. Collier, *White book ELI: Extreme Light Infrastructure, Science and Technology with Ultra-Intense Lasers* (Andreas Thoss, Berlin, 2011).
12) The Institute of Applied Physics, the Russian Academy of Sciences, Exawatt Center for Extreme Light Studies (XCELS) [http://www.xcels.iapras.ru/].
13) D. Strickland and G. Mourou, Opt. Commun. **56**, 219 (1985).
14) A. Dubietis, G. Jonušauskas, and A. Piskarskas, Opt. Commun. **88**, 437 (1992).
15) J. Ren, W. Cheng, S. Li, and S. Suckewer, Nat. Phys. **3**, 732 (2007).
16) N. Stuart, T. Robinson, D. Hillier, N. Hopps, B. Parry, I. Musgrave, G. Nersisyan, A. Sharba, M. Zepf, and R. A. Smith, Opt. Lett. **41**, 3221 (2016).
17) S. Kane and J. Squier, J. Opt. Soc. Am. B **14**, 1237 (1997).
18) D. N. Schimpf, E. Seise, J. Limpert, and A. Tünnermann, Opt. Express **16**, 8876 (2008).
19) H. Ren, L. Qian, H. Zhu, D. Fan, and P. Yuan, Opt. Express **18**, 12948 (2010).
20) J. Bromage, C. Dorrer, and R. K. Jungquist, J. Opt. Soc. Am. B **29**, 1125 (2012).
21) C. Dorrer, J. Opt. Soc. Am. B **24**, 3048 (2007).
22) D. N. Schimpf, E. Seise, J. Limpert, and A. Tünnermann, Opt. Express **16**, 10664 (2008).
23) M. Iliev, A. K. Meier, B. Galloway, D. E. Adams, J. A. Squier, and C. G. Durfee, Opt. Express **22**, 17968 (2014).
24) F. Tavella, A. Marcinkevičius, and F. Krausz, New J. Phys. **8**, 219 (2006).
25) C. Homann and E. Riedle, Laser Photonics Rev. **7**, 580 (2013).
26) J. Moses, S.-W. Huang, K.-H. Hong, O. D. Mücke, E. L. Falcão-Filho, A. Benedick, F. Ö. Ilday, A. Dergachev, J. A. Bolger, B. J. Eggleton, and F. X. Kärtner, Opt. Lett. **34**, 1639 (2009).
27) K. Kondo, H. Maeda, Y. Hama, S. Morita, A. Zoubir, R. Kodama, K. A. Tanaka, Y. Kitagawa, and Y. Izawa, J. Opt. Soc. Am. B **23**, 231 (2006).
28) J. Wang, J. Ma, Y. Wang, P. Yuan, G. Xie, and L. Qian, Opt. Lett. **39**, 2439 (2014).
29) Z. Li, S. Tokita, S. Matsuo, K. Sueda, T. Kurita, T. Kawasima, and N. Miyanaga, Opt. Express **25**, 21201 (2017).
30) R. C. Shah, R. P. Johnson, T. Shimada, K. A. Flippo, J. C. Fernandez, and B. M. Hegelich, Opt. Lett. **34**, 2273 (2009).
31) Z. Li, K. Tsubakimoto, H. Yoshida, T. Uesu, K. Tsuji, and N. Miyanaga, Opt. Express **25**, 7465 (2017).
32) A. Jullien, O. Albert, F. Burgy, G. Hamoniaux, J. Rousseau, J. Chambaret, F. Augé-Rochereau, G. Chériaux, J. Etchepare, N. Minkovski, and S. M. Saltiel, Opt. Lett. **30**, 920 (2005).
33) P. Yuan, G. Xie, D. Zhang, H. Zhong, and L. Qian, Opt. Lett. **35**, 1878 (2010).
34) J. Liu, K. Okamura, Y. Kida, and T. Kobayashi, Opt. Express **18**, 22245 (2010).
35) I. Musgrave, W. Shaikh, M. Galimberti, A. Boyle, C. Hernandez-Gomez, K. Lancaster, and R. Heathcote, Appl. Opt. **49**, 6558 (2010).
36) H. Kiriyama, T. Shimomura, H. Sasao, Y. Nakai, M. Tanoue, S. Kondo, S. Kanazawa, A. S. Pirozhkov, M. Mori, Y. Fukuda, M. Nishiuchi, M. Kando, S. V. Bulanov, K. Nagashima, M. Yamagiwa, K. Kondo, A. Sugiyama, P. R. Bolton, T. Tajima, and N. Miyanaga, Opt. Lett. **37**, 3363 (2012).
37) A. Yogo, K. Kondo, M. Mori, H. Kiriyama, K. Ogura, T. Shimomura, N. Inoue, Y. Fukuda, H. Sakaki, S. Jinno, M. Kanasaki, and P. R. Bolton, Opt. Express **22**, 2060 (2014).
38) S. Liang, H. Liu, N. Huang, Q. Sun, Y. Wang, and W. Zhao, Opt. Lett. **37**, 241 (2012).
39) D. Kaganovich, J. R. Peñano, M. H. Helle, D. F. Gordon, B. Hafizi, and A. Ting, Opt. Lett. **38**, 3635 (2013).
40) A. Gatti, H. Wiedemann, L. A. Lugiato, I. Marzoli, G.-L. Oppo, and S. M. Barnett, Phys. Rev. A **56**, 877 (1997).
41) A. Gatti, L. A. Lugiato, G.-L. Oppo, R. Martin, P. Di Trapani, and A. Berzanskis, Opt. Express **1**, 21 (1997).
42) T. Kawashima, T. Kanabe, O. Matsumoto, R. Yasuhara, H. Furukawa, M. Miyamoto, T. Sekine, T. Kurita, H. Kan, M. Yamanaka, M. Nakatsuka, and Y. Izawa, Electr. Eng. Jpn. **155** [2], 27 (2006).
43) T. Kurita, K. Sueda, T. Sekine, T. Kawashima, and N. Miyanaga, J. Phys.: Conf. Ser. **244**, 032009 (2010).
44) N. V. Didenko, A. V. Konyashchenko, A. P. Lutsenko, and S. Yu. Tenyakov, Opt. Express **16**, 3178 (2008).